Theoretical and experimental electronic distributions in AL_6Mn

1993 J. Phys.: Condens. Matter 5 3339

(http://iopscience.iop.org/0953-8984/5/20/007)

J. Phys.: Condens. Matter 5 (1993) 3339–3350. Printed in the UK

Theoretical and experimental electronic distributions in Al_6Mn

Zoltán Dankházi†‡, Guy Trambly de Laissardière§, Duc Nguyen Manh§, Esther Belin† and Didier Mayou§

† Laboratoire de Chimie Physique Matière et Rayonnement URA 176 and GDR 5, 11 rue Pierre et Marie Curie, 75231 Paris Cédex 05, France
§ LEPES-CNRS and GDR 5, 25 Avenue des Martyrs, BP 166X, 38042 Grenoble, France
‡ Institut for Solid State Physics, Eötvös University, Muzeum korút 6-8, 1088 Budapest, Hungary

Received 4 January 1993, in final form 8 February 1993

Abstract. We report on a comparison between densities of states of crystalline Al_6Mn calculated using the LMTO band structure method and electronic distributions obtained by means of soft x-ray spectroscopy experiments. The agreement is found to be rather good. We propose that changes in Al sites are responsible for the modifications of the densities of states observed in quasicrystalline Al–Mn alloys.

1. Introduction

The discovery in 1984 of fivefold rotational symmetry in rapidly quenched alloys has given impulse to numerous investigations of the atomic and electronic structures of this new class of materials, so-called quasicrystals, and also to comparisons with crystalline alloys of related nominal composition.

Many systems of this new class of solids are alloys of elements with small differences in radii and electronegativities and they are considered as Hume-Rothery alloys (Friedel and Dénoyer 1987). At an experimental level, this is confirmed by x-ray diffraction patterns which show that Bragg planes of spots with high intensities are near the Fermi surface (Matsuo *et al* 1989). This diffraction by Bragg planes is well known to create a pseudo-gap near the Fermi level (E_F) and one can expect that crystalline phases of composition close to that of quasicrystals may have also a pseudo-gap near E_F. This however has to be checked by experimental and theoretical means. Another interesting aspect is the hybridization between sp and d states which tends to increase the pseudo-gap and can lead to a splitting of the d bands (Trambly de Laissardière *et al* 1993, Fujiwara and Yokokawa 1991).

In order to explore these effects, we have undertaken experimental investigations and *ab initio* calculations using the linear muffin tin orbital (LMTO) method. Note that we have already reported experimental results obtained using soft x-ray and photoelectron spectroscopies (respectively SXS and XPS) which concern both valence and conduction state distributions in a series of quasicrystalline and crystalline alloys of various compositions, where we actually find evidence for low DOSs at the Fermi level and the formation of a pseudo-gap (Traverse *et al* 1988, Belin and Traverse 1991, Belin *et al* 1991, 1992).

0953-8984/93/203339+12$07.50

In the present paper, we focus mainly on a crystalline Al–Mn alloy, namely Al_6Mn, with the aim of comparing partial occupied and unoccupied densities of states (DOS) as calculated in the LMTO framework with experimental electronic distributions. The paper is organized in the following way: in the first section we summarize the principle of the calculation and detail the results for the partial DOSs; in the second section we recall the principle of the experimental SXS and XPS techniques and the previous results which we have obtained for Al_6Mn (Traverse *et al* 1988, Belin and Traverse 1991, Belin *et al* 1991); finally we compare and discuss the theoretical and experimental data in the third section. In this last section, we also present a brief comparison between crystalline Al_6Mn and quasicrystalline Al–Mn alloys.

2. Calculations

We have performed a self-consistent scalar–relativistic LMTO calculation in the atomic sphere approximation (ASA) (Andersen *et al* 1985, 1987) for Al_6Mn. We used the cubic-face-centred orthorhombic structure with the experimental lattice constants: $a = 7.5518$ Å, $b = 6.4978$ Å and $c = 8.8703$ Å (*Cmcm* space group) (Nicol 1953). The unit cell contains 28 atoms (figure 1) to which correspond four different Wyckoff positions displayed in table 1 (Pearson 1985). Details for the interatomic distances derived from experiments are given in table 2. The most interesting features are (i) the small interatomic distance between the manganese and the Al (2) atoms and (ii) the very short distances between Al (2)–Al (2) atoms. The Mn (c) atoms have coordination 10 and are surrounded only by Al atoms as follows: two Al (2), four Al (3) and four Al (1). The average Mn–Al and Al–Al distances are 2.56 Å and 2.78 Å respectively.

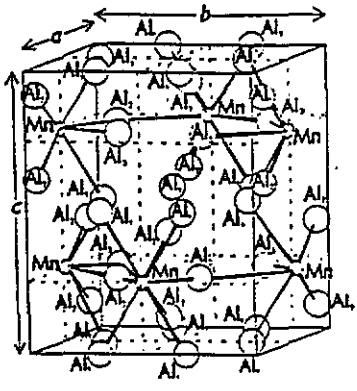

Figure 1. Distribution of Al and Mn atoms in the unit cell of crystalline Al_6Mn as taken from Nicol (1953).

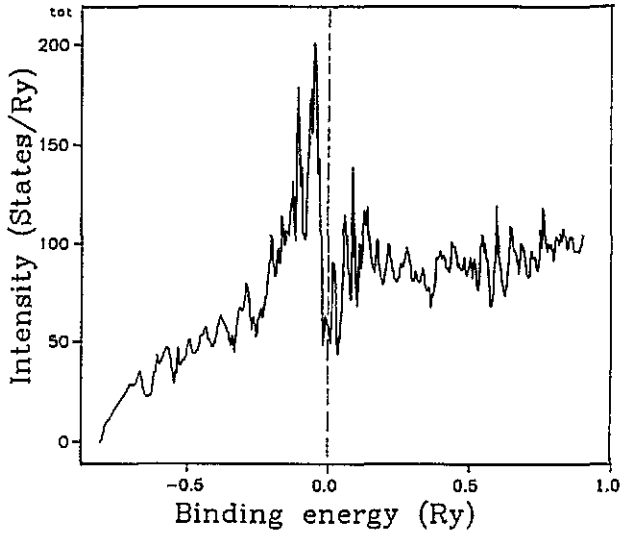

Figure 2. Total Al_6Mn DOS calculated within the LMTO framework.

Table 1. Wyckoff positions of the different Al sites in crystalline Al_6Mn (Villars and Calvert 1985).

Atom	Wyckoff notation	x	y	z
Al (1)	8(e)	0.324	0	0
Al (2)	8(f)	0	0.1402	0.1020
Al (3)	8(g)	0.317	0.2838	0.25
Mn	4(c)	0	0.4567	0.25

Table 2. Interatomic distances in crystalline Al_6Mn.

Atom	Neighbour	Number of atoms	Distance (Å)
Mn	Al (1)	4	2.6
	Al (2)	2	2.435
	Al (3)	2	2.64
	Al (3)	2	2.54
Al (1)	Mn	2	2.60
	Al (1)	1	2.64
	Al (2)	2	2.76
	Al (2)	2	2.84
	Al (3)	2	2.84
	Al (3)	2	2.88
Al (2)	Mn	1	2.435
	Al (1)	2	2.76
	Al (1)	2	2.84
	Al (2)	1	2.57
	Al (2)	1	2.62
	Al (3)	2	2.89
	Al (3)	2	2.77
Al (3)	Mn	1	2.64
	Mn	1	2.54
	Al (1)	2	2.84
	Al (1)	2	2.88
	Al (2)	2	2.89
	Al (2)	2	2.77
	Al (3)	1	2.77

The calculation uses the atomic sphere approximation in which the sphere radii are chosen so that the total volume of the spheres equals that of the solid. In our calculations the sphere radii are $R_{Al} = 1.59$ Å and $R_{Mn} = 1.50$ Å. This leads to a radius ratio $R_{Mn}/R_{Al} = 0.94$ and an overlap between neighbouring spheres of 30% which is reasonable in LMTO calculation (Andersen *et al* 1985, 1987). Let us emphasize that this choice corresponds to the minimal excess numbers of electrons in each atomic sphere which cannot, in general, be considered as physically significant and cannot be called 'charge transfer' (Nguyen Manh *et al* 1992).

We used a scalar relativistic LMTO–ASA code (Christensen 1985) with the combined corrections which account for the finite number of terms in the angular momentum expansions; note that we include here terms with $l \leqslant 2$ which means that the Al (3s, 3p, 3d) and Mn (4s, 4p, 3d) levels are treated as valence states. The density functional formalism was treated within the local density approximation with the exchange and correlation potential of von Barth and Hedin (1972).

The self-consistent electronic structure was obtained from a grid of 105 irreducible k points (i.e. 512 k points in the Brillouin zone). The eigenvalues were used to calculate the DOSs with the tetrahedron method. We have performed the total energy calculation for different volumes with the experimental ratios of b/a and c/a and obtained the value of lattice constant $a = 7.408$ Å. From this dependence, we calculated the bulk moduli and obtained the value of 1.21 mb. The self-consistency process was stopped when the total energy of all the atoms was changed by less than 10^{-2} mRyd per iteration.

We present in figure 2 the total Al_6Mn DOS which we have obtained. Both the occupied and unoccupied DOSs (respectively VB and CB) exhibit a spiky shape; intense VB states of about 200 states Ryd^{-1} are present near E_F and there is a narrow pseudo-gap at E_F. Table 3 indicates the values of the DOSs at E_F. Let us recall that Fujiwara (1989, 1990) already concluded from a DOS calculation for a cubic $Al_{114}Mn_{24}$ cluster analogous to quasicrystals that spiky DOS should be a common feature in crystalline and quasicrystalline Al–Mn alloys.

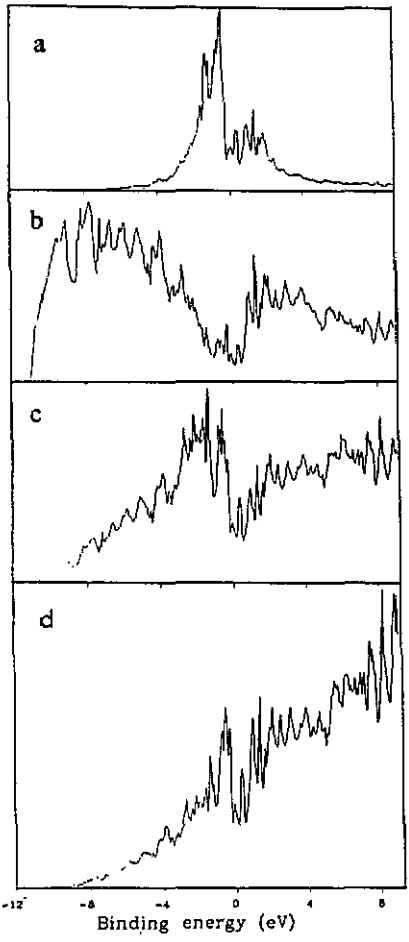

Figure 3. Partial Mn d (a), Al s (b), Al p (c) and Al d (d) DOS curves. For Al, these curves refer to the sum of the contributions of the different Al sites in the crystal.

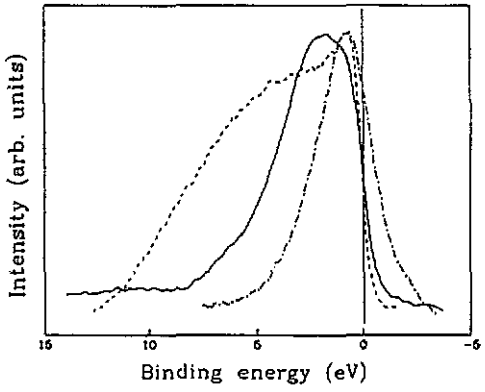

Figure 4. Valence band of crystalline Al_6Mn. The full line refers to Al 3p states, the short dotted line to Al 3s–d states and the long dashed dotted line to Mn 3d states. The curves are arbitrarily normalized to their maximum intensity.

Table 3. Al and Mn s, p and d DOSs at E_F in states Ryd^{-1}.

	Al				
	Site 1	Site 2	Site 3	All Sites	Mn
s	1.256 17	0.508 021	1.438	3.202 191	0.314 595
p	6.997 26	5.335 99	4.341 67	16.674 92	1.610 56
d	3.199 23	4.336 28	3.045 91	10.581 42	26.5373

The partial DOSs are displayed in figures 3(*a*), (*b*), (*c*) and (*d*). Let us mention that in the LMTO method, it is well known that partial DOSs on one site can be influenced by states which are centred on neighbouring spheres and, therefore, it is difficult to define strictly a partial DOS on one single site. The Mn d DOSs curve given figure 3(*a*) is spiky and intense below E_F in the VB region, these Mn VB d states, of about 100 states Ryd^{-1}, which are the dominant states of the total DOSs extend over about 1.5 eV. A pseudo-gap is present at E_F about in the middle of the total d band. Let us mention that Mn p and s states do not significantly contribute to the VB since their maximum is about 3% that of the Mn d states.

We show in figures 3(*b*), 3(*c*) and 3(*d*) the partial Al s, p and d DOS curves which correspond to the sum of the contributions of all the different Al sites. All these curves are quite spiky. In the VB, there are very few Al s states near E_F since they concentrate mainly in the range between +3 and +11 eV from E_F; the s states overlap d states between +2 and +4 eV so they are slightly s–d hybridized except close to E_F; the s states rather overlap p states and thus are s–p hybridized in the energy range +2 to +8 eV; in the high binding energy region of the DOS curve the states are almost pure Al s, and their maximum intensity is about 33 states Ryd^{-1}. The Al p states spread over about 3.5 eV; in the corresponding DOS curve, the spikes are distributed roughly around a parabola-like mean curve except in the range within +3 eV from E_F where the intensity enhances and the curve displays an intense two peaked structure. These two peaks are denoted A and B; the most intense one, which corresponds to about 75 states Ryd^{-1}, is located at about +1.4 eV and the other one is at +0.7 eV. The Al VB d states are mainly located in the energy range which covers +3.5 eV from E_F, and exhibit two principal peaks labelled A′ and B′ situated at +0.6 and +1.4 eV, with maximum intensity about 29 states Ryd^{-1}. From the overlap between the various Al p and d DOSs VB curves in the region involving $E_F+1.5$ eV we deduce that there is a significant Al p–d hybridization in crystalline Al_6Mn. This hybridization is stronger in the energy range involving features A/A′, i.e. at about $E_F + 0.7$–0.9 eV.

In the CB energy range, the curves corresponding to Al p, d and s DOS (figures 3(*b*), (*c*) and (*d*)) overlap. So, the conduction Al states are s–p–d hybridized over 4 eV beyond E_F and after that more p–d hybridized until about −8 eV. The CB part of Mn d curve (figure 3(*a*)) overlaps the others in the range E_F–3 eV so the Al s–p–d hybridized states interact with Mn d states over this energy range.

3. Experimental details

We have used homogeneous single-phase samples as checked by transmission electron microscopy which were prepared by either ion beam mixing of thin Al and Mn layers (Traverse *et al* 1988) or by the classical rapid solidification technique.

The experiments have been carried out by means of soft x-ray emission spectroscopy (SXES) and soft x-ray absorption spectroscopy (SXAS). Let us recall that these two techniques

involve respectively transitions between an inner level and either the valence or conduction bands; thus they provide separate information on occupied and unoccupied electronic distributions which are partial since the x-ray transitions are governed by dipole selection rules and are local because the inner level belongs to a given component of the solid. Thus, the measured spectral intensities are proportional to the partial DOS convoluted by the energy distribution of the inner level which is involved in the x-ray transition. Moreover, the x-ray transitions are dependent on the transition probabilities, and these are usually constant or vary slowly as a function of energy in the spectral range analysed; note that, because of these transition probabilities, when the inner level hole is p-like, transitions from (or to) states with d character are favoured with respect to those from (or to) s character. So, the shapes of the experimental x-ray spectra are directly related to those of the DOSs. However, since the electronic distribution curves are normalized to their respective maximum intensity in the case of SXES experiments, no absolute DOS values can be derived from the experiments but comparison between curves of same spectral character in various samples is possible.

From x-ray photoelectron spectroscopy experiments, binding energies are obtained, making it possible to measure those corresponding to the inner levels involved in the x-ray transitions. It follows that we can locate the Fermi level on the various x-ray transition energy scales and that the different partial electronic distributions can be adjusted in the binding energy scale (BE) by taking the Fermi level position as the origin. Consequently, combining the results of SXS and XPS allows direct comparison of the various electronic distributions in BE, providing insight into the electronic interactions and describing both VB and CB.

Figure 4 shows the result of the adjustment of the experimental curves corresponding to Mn 3d, Al 3p and Al 3s–d states distributions for Al_6Mn. As already discussed elsewhere (Belin *et al* 1992), this points out that Mn d states are located close to the Fermi level in interaction with Al s–dp hybridized states, Al s–p states are found in the middle of the VB while the high binding region is almost Al s-like.

4. Discussion

We have recalled above that the experimental curves reflect the product $|M|^2$. $N(E) * L(E)$ where M is the matrix element of the transition probability, $N(E)$ is the partial DOS and $L(E)$ a Lorentzian function whose full width at half maximum intensity (FWHM) is the energy width of the inner level involved in the x-ray transition. We also mentioned that in general, the transition probabilities are nearly constant in the energy range investigated. So, to compare the theoretical results with the experimental ones, we simulated theoretical x-ray spectra as follows: we broadened each partial calculated DOS by a convenient function L and, to account for the instrumental functions of our apparatus, we have smoothed out the result with suitable Gaussian functions, G. The widths of the functions L and G are given in table 4. The final results for the Al_6Mn VB are displayed in figures 5(a), (b) and (c) respectively together with the Mn 3d, Al 3p and Al 3s–d experimental curves.

The Mn 3d simulated curve is displayed in figure 5(a). Its FWHM is 2.5 ± 0.1 eV, the maximum is at $+0.9 \pm 0.1$ eV and the intensity at E_F is 56% that of the maximum. These values are respectively 3.0 ± 0.1 eV, $+0.8 \pm 0.1$ eV and 79% in the experiment. The Mn 3d spectrum in the one-electron model is produced by the decay of a 3d VB electron to the $2p_{3/2}$ hole. In fact, during the experiment, the spectrum is excited with photons of energy higher than that strictly necessary to create a single hole in the $2p_{3/2}$ inner level. It turns out that multiple ionizations are generated and thus satellite lines, wider than the principal one and

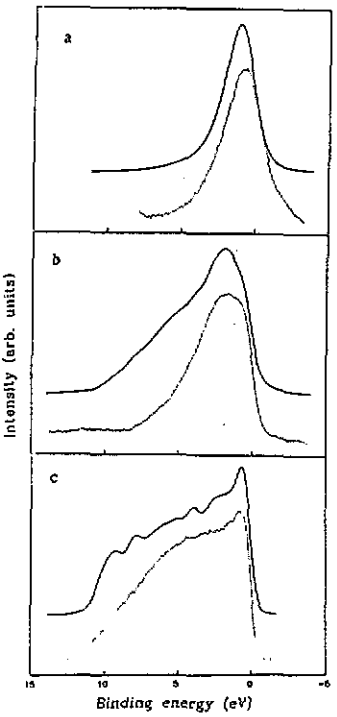

Figure 5. (*a*) Mn 3d simulated (full line) and experimental (dotted line) curves. (*b*) Al 3p simulated (full line) and experimental (dotted line) curves. (*c*) Al 3(s+1.9 d) simulated (full line) and experimental (dotted line), curves.

Table 4. FWHM of the Lorentzian distribution (L) corresponding to the inner levels involved in the x-ray transitions and of the Gaussian distribution (G) for the instrumental functions.

	L_{VB}	G_{VB}	L_{CB}	G_{VB}
Mn d	0.5	0.5		
Mn p			1.3	0.5
Al p	0.5	0.2	0.5	0.5
Al d	0.1	0.3		
Al s	0.1	0.3		

located at lower BE, are emitted during the x-ray process; the result of this many-body effect is to shift somewhat the maximum and broaden the spectral distribution mainly towards low BE and so slightly enhance the intensity at E_F with respect to the expected value within the one-electron approximation. Once accounting for this experimental artefact, there is a fair agreement between the results of experiment and theory.

The Al 3p distributions are shown in figure 5(*b*). The intensity at E_F is about 96±4% of that corresponding to pure Al. The calculated curve is wider here than the experimental one towards high BE, and the edge close to E_F is less steep and the states near E_F, over about 1.5 eV, are less populated than in the experiment. We have already emphasized that near E_F there is a p–d hybridization and that the states from +4 eV to high BE are principally s–p hybridized. The discrepancies observed between experiment and calculation might be overcome with a slight modification of the p states distribution by somewhat increasing p–d and decreasing s–p hybridizations. Indeed, on doing so, the states near the edge increase in intensity and the edge itself straightens up and becomes closer to the Fermi level, at the same time the high-bonded p states become less intense. Let us recall that the maximum of

the Al p states distribution is split into two parts (denoted (a) and (b) on the figure) which correspond within the experimental accuracy to the peaks A, A′ and B, B′ of the calculated p and d DOS curves.

Concerning Al s–d VB states distributions, whose intensity at E_F is about $92 \pm 4\%$ of that corresponding to pure Al, we display in figure 5(c) the experimental curve and compare with the calculated curve, which results from the sum of the s and d DOSs contributions corresponding to all the Al sites. In order to simulate the experimental curve, we assign to the d DOS contribution a higher weighting than the s DOSs because the transition probabilities favour transitions from d states with respect to s ones. The best fit to the experiment is obtained for (s+1.9 d) broadened calculated DOSs. Here also, we observe a discrepancy between calculation and experiment: the intensity of high binding energy calculated states (beyond +4 eV) is overestimated compared to the experiment and there are two features located at about +7 and +8.5 eV from E_F which are not present in the experimental result. However, note that the experimental edge is very well fitted by the calculation. This emphasizes that at E_F, there should actually be almost pure d states, which are underestimated by the calculation and that s–d hybridization exists only over the energy range beyond $\simeq +2$ eV.

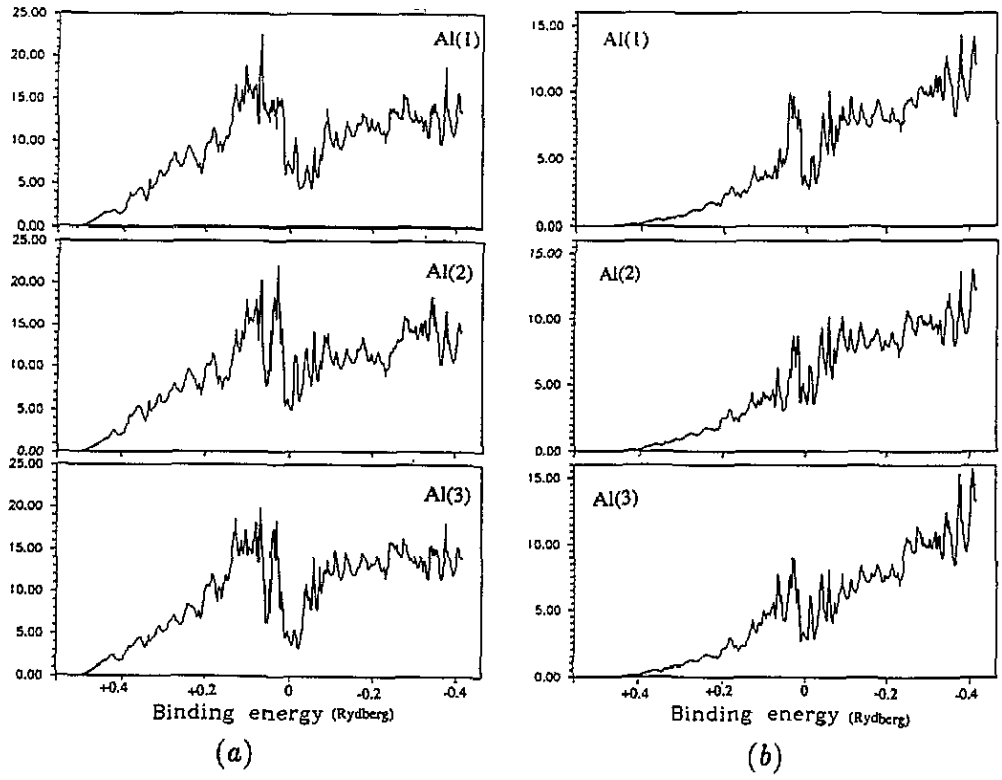

Figure 6. (a) left side = Al p partial DOSs as calculated within the LMTO framework for the different Al (1), Al (2) and Al (3) sites. (b) right side = Al d partial DOSs as calculated within the LMTO framework for the different Al (1), Al (2) and Al (3) sites.

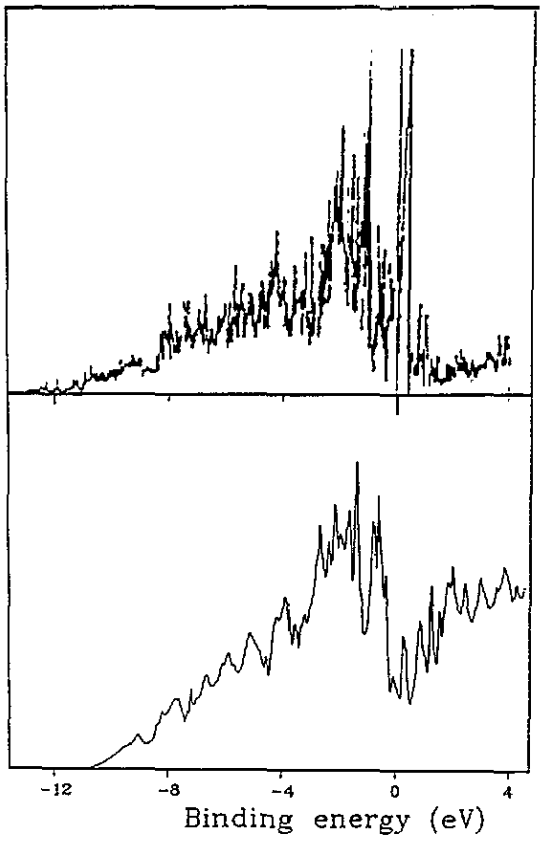

Figure 7. Total partial Al p DOSs: lower curve, this work; upper curve, from Fujiwara (1989, 1990).

Let us mention two other effects which could contribute to the slight discrepancies we observe. Firstly, as already mentioned above, in the LMTO method the partial DOSs on one site can be influenced by states which are centred on neighbouring spheres. Secondly, the experimental results give the partial DOS provided that the square matrix element $|M|^2$ is nearly constant. Indeed, from model calculations of Trambly de Laissardière *et al* (1993), it is clear that eigenstates are linear combinations of several plane waves. As a result, an eigenstate $\Phi(E, r)$ of energy E, $\Phi(E, r)^2$ varies rapidly with position and energy. This could lead to some variation of the matrix element $|M|^2$ with energy and thus to some discrepancies in the composition between theory and experiment.

We will not discuss in detail here the CB states distribution, let us simply recall that Al p and Mn p distribution curves both exhibit a $\tan^{-1}$-like edge in the vicinity of E_F followed by a structureless plateau or a monotonic increase of intensity (Belin *et al* 1992). These results are in full agreement with the curves simulated from the theoretical results.

Finally, despite the observed discrepancies in occupied states distributions which we discussed above, there is a satisfactory qualitative agreement between experimental VB and CB states distribution and calculation.

In the VB energy range close to E_F, the Al p–d hybridization seems to play an important role in Al–Mn alloys; in particular, it seems to be quite sensitive to the structural arrangement

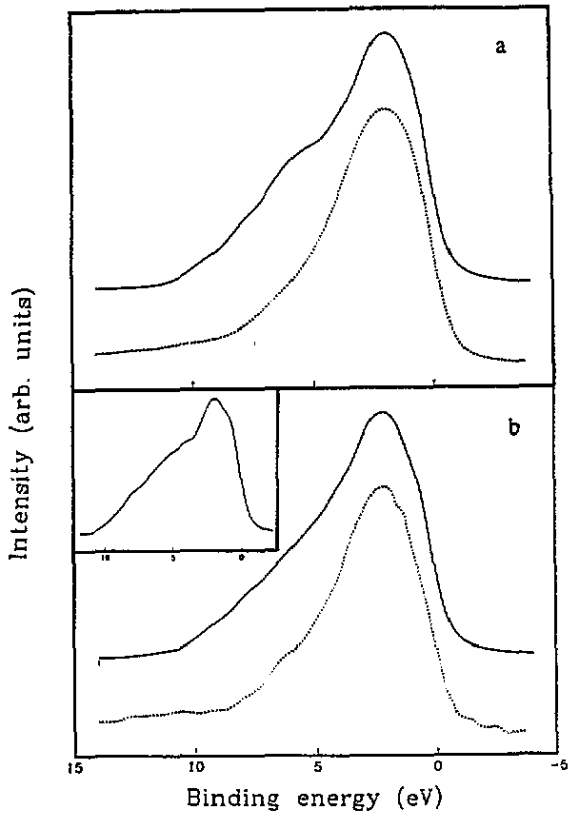

Figure 8. Comparison between the calculated broadened partial DOSs curves and experimental results. (*a*) Calculated curve for site Al (1) (full line) and the experimental Al p DOSs curve for quasicrystalline icosahedral phase (dotted line). (*b*) calculated curve for site Al (3) (full line) and the experimental Al p DOSs curve for quasicrystalline decagonal phase (dotted line). The calculated curve for site Al (2) is given in the insert of figure 8(*b*).

of the alloys. Indeed, when going from crystalline to icosahedral (I) and to decagonal (T) quasicrystalline phases it has been evidenced and reported previously (Traverse *et al* 1988, Belin and Traverse 1991, Belin *et al* 1991), that (i) the Al DOS at E_F decreases in the quasicrystals with respect to the corresponding crystal (ii) the edge of the Al 3p states distribution is less steep and bends towards high BE in the quasicrystals as compared to the crystalline phases, and this effect is more marked for T than I quasicrystals, (iii) there is a modification of the shape of the Al 3p curve in the energy range of the maximum distribution: this one is rounded for the I phase and split into two parts for the T phase. So the relevant result is that there is a progressive depopulation of VB states in the range E_F to +2 eV in T and I phases as compared to the crystals.

For Al_6Mn, our calculations point out that in the partial p and d DOSs for the various Al sites: (i) the p DOSs are stronger for Al (2) and Al (3) sites than for site Al (1), (ii) the partial Al d DOSs are decreased in Al (2) and Al (3) sites with respect to the site Al (1) (figures 6(*a*) and (*b*)); note that the p DOSs are twice or thrice higher than the d DOSs. Therefore differences exist in the p–d hybridization according to the Al site.

Let us recall that Fujiwara (1989, 1990) has calculated total and partial DOS using the

LMTO approximation for a cubic $Al_{114}Mn_{24}$ cluster simulating the local order of the I-Al–Mn quasicrystalline phase. We show in figure 7 Fujiwara's result for the partial Al p DOS. The corresponding curve is very spiky. However, near E_F, there are two principal structures denoted α and β which are located at approximately +0.7 and +1.2 eV. These structures are analogous to the peaks A and B of our Al p DOS curve for Al_6Mn. The intensity of feature B with respect to A is higher than that of feature β with respect to α (figure 7(*b*)). This result together with our own calculation lead us to suggest that in I and T quasicrystals, the depopulation of VB in the region near E_F could be the consequence of a drastic decrease of the strength of the Al p–d hybridization with respect to the crystalline alloys. This could be due to partial Al p and Al d DOSs modifications near E_F when changing the atomic structure. Indeed, let us consider the partial Al p DOSs and broaden them by functions L and G as indicated previously. For site Al (1), a curve with a rounded shape is obtained. For site Al (2), the curve displays two well resolved peaks, the narrowest being closer E_F. For the site Al (3), the curve also displays two peaks; the one close to E_F is less intense and the edge itself is less steep than for Al (2). We propose the structural change from crystal to quasicrystal might be due to the presence in the I quasicrystals mainly of Al sites analogous to the Al (1) sites of Al_6Mn while in T alloys there might be mainly Al (3)-like sites with possibly a few Al (1) and Al (2)-like sites. We show in figure 8(*a*) and (*b*) the comparison between the experimental Al p DOSs curves for I and T phases and the calculated broadened partial DOSs curves of sites Al (1) and Al (3). The curve for site Al (2) is given in the insert.

Note that the framework of our suggestion the progressive repulsion from E_F of the Al valence band edge (which has been demonstrated in Al–Mn quasicrystals when comparing to crystalline alloys of same or close nominal composition (Traverse *et al* 1988, Belin and Traverse 1991)) results from the decrease of Al p states near E_F as a consequence of the modification of the kind of Al sites.

Acknowledgments

We would like to express our gratitude to Professor D A Papaconstantopoulos for his interest in the work and for his comments on the manuscript. We are indebted to Professor T Fujiwara for stimulating discussions. One of us (ZD) acknowledges financial support from a TEMPUS contract No HUS-017-91 and a BGF No 92/108.

References

Andersen O K, Jepsen O and Glotzet D 1985 *Highlights of Condensed Matter Theory* ed F Bassani, F Fumi and M P Tosi (New York: North-Holland)

von Barth U and Hedin L 1972 *J. Phys. C: Solid State Phys.* **5** 1629

Belin E, Dankhazi Z, Sadoc A, Calvayrac Y, Klein T and Dubois J M 1992 *J. Phys.: Condens. Matter* **4** 4459

Belin E, Kojnok J, Traverse A, Harmelin M, Berger C and Dubois J M 1991 *J. Phys.: Condens. Matter* **4** 1057

Belin E and Traverse A 1991 *J. Phys.: Condens. Matter* **3** 2157

Christensen N E 1985 *Phys. Rev.* B **32** 207

Friedel J and Dénoyer F 1987 *C. R. Acad. Sci., Paris* T **305** 171

Fujiwara T 1989 *Phys. Rev.* B **40** 942

—— 1990 *Solid State Commun.* **117–8** 844

Fujiwara T and Yokokawa T 1991 *Phys. Rev. Lett.* **66** 333

Matsuo S, Nakano H, Ishimasa T and Fukano Y 1989 *J. Phys.: Condens. Matter* **1** 6893

Nguyen Manh D, Trambly de Laissardière G, Julien J P, Mayou D and Cyrot-Lackmann F 1992 *Solid State Commun.* **82** 329

Nicol A I D 1953 *Acta Crystallogr.* **6** 285

Trambly de Laissardière G, Mayou D and Nguyen Manh D 1993 *Europhys Lett.*

Traverse A, Dumoulin L, Belin E and Sénémaud C 1988 *Quasicrystalline Materials (Institut Laue–Langevin CODEST Workshop)* ed C Janot and J M Dubois (Singapore: World Scientific) p 399

Villars P and Calvert L D 1985 *Pearson's Handbook of Crystallographic Data for Intermetallic Phases* vol I (Warrendale, PA: American Society for Metals)